Journal of Membrane Science 666 (2023) 121148

Contents lists available at ScienceDirect

Journal of Membrane Science

journal homepage: www.elsevier.com/locate/memsci

Designing monovalent selective anion exchange membranes for the simultaneous separation of chloride and fluoride from sulfate in an equimolar ternary mixture

Önder Tekinalp [a], Pauline Zimmermann [b], Odne Stokke Burheim [b], Liyuan Deng [a,*]

[a] Department of Chemical Engineering, Norwegian University of Science and Technology (NTNU), NO-7491, Trondheim, Norway
[b] Department of Energy and Process Engineering, Norwegian University of Science and Technology (NTNU), NO-7491, Trondheim, Norway

ARTICLE INFO

Keywords:
Electrodialysis
Monovalent selectivity
Anion exchange membranes
Hydrophobicity
Layer-by-layer deposition

ABSTRACT

Selective removal of multiple counter-ions in a single mixture is highly desirable for many industrial applications but also very challenging. This study focuses on designing monovalent selective anion exchange membranes (AEMs) for the simultaneous separation of F^- and Cl^- from SO_4^{2-} using electrodialysis (ED). A series of brominated poly(2,6-dimethyl-1,4-phenylene oxide) (BPPO) polymers with adjusted bromination degrees at benzyl and aryl positions were synthesized, and quaternized with different tertiary amines of varying chain lengths to produce optimized AEMs. Differences in bromination degrees and the chain lengths of the tertiary amines alter the microstructure of AEMs, which influences the anion transport through the developed membranes. Selected AEMs were modified via layer-by-layer (LbL) deposition of poly (sodium 4-styrenesulfonate) (PSS) and poly (allylamine hydrochloride) (PAH) polyelectrolytes to enhance their monovalent selectivity. ED tests were carried out with an equimolar ternary mixture. When 5 layers of deposition were applied, the achieved Cl^-/SO_4^{2-} and F^-/SO_4^{2-} selectivities were 11.7 ± 0.2 and 8.3 ± 0.3, respectively, showing significant improvement compared to a commercial monovalent selective ASVN membrane. Experimental results confirm that simultaneously optimizing membrane microstructure and surface can be an effective strategy for the separation of similar counter-ions in an ED process.

1. Introduction

Demands for separating halide anions have considerably increased from various industrial applications, especially during the recent decade [1]. Specifically, there is a particular need to remove excess F^- and Cl^- from SO_4^{2-} based solutions, such as groundwater treatment, hydrometallurgical applications, or thermal power generation processes, as the toxicity and corrosivity of these halide anions not only pose harm to terrestrial and aquatic life but also threaten the working environment and process equipment [2–4]. Electrodialysis (ED) is an ion exchange membrane (IEM) based technology for purifying such solutions [5]. By applying an electric potential across the cell in ED, electrochemical reactions occur at the electrodes that deplete or create ions, causing a charge imbalance and the formation of an electric field across the cell. As a result, cations migrate towards the cathode, passing through the cation exchange membrane (CEM), and reciprocally, anions migrate towards the anode, transferring through the anion exchange membrane (AEM) [6].

Using IEM in an ED process is advantageous because it offers higher selectivity and capacity, and is an environmentally friendly process with lower energy consumption than other purification processes for the same separation, such as nanofiltration, reverse osmosis, precipitation, and adsorption [7,8]. Standard commercial IEMs have been used to separate counter-ions and co-ions. However, in general, selectivity among different species of counter-ions in a single solution is not sufficient, which restricts the broad applicability of IEMs for potential industrial applications, *e.g.,* acid recovery in hydrometallurgy, lithium recovery from brine, and sodium chloride production from seawater [9]. Therefore, strategies to enhance the selectivity of ion(s) of a given charge over other ions of the same charge are highly desirable. The selectivity of ions is mainly determined by the valency and size of the ions and membrane properties, which affect: *i)* the affinity of ions at the surface for fixed charged groups in the IEM, *ii)* the ingress rate of ions to

* Corresponding author.
E-mail address: liyuan.deng@ntnu.no (L. Deng).

https://doi.org/10.1016/j.memsci.2022.121148
Received 11 September 2022; Received in revised form 21 October 2022; Accepted 31 October 2022
Available online 11 November 2022

the membrane, where the dimensions of the hydrophilic entrance into the IEM are typically sub-nanometer, with smaller ions entering much faster than larger ions, and *iii)* the mobility of ions in the membrane influenced by the nature of the ionic pathway present in the membrane (i.e., tortuosity, dimensions, hydrophobicity/hydrophilicity) [10,11]. Hence, designing IEMs' matrix and surface in favor of target ions' characteristics is the key to enhance the selectivity among counter-ions of different or equal valency.

One strategy to adjust the ions' affinity and mobility with a membrane is to introduce hydrophobic side-chains into the membrane structure [10,15]. A side-chain-type IEMs can offer prominent hydrophilic/hydrophobic discrimination between the flexible functionalized segments and unfunctionalized backbones, yielding a micro-phase separated structure [16]. This structure triggers the dehydration of ions of lower hydration energy, whereas ions of higher hydration energy are impeded by the hydrophobic structure. Some examples of side-chain-type homogenous AEMs have recently been reported to explore their applications to the $Cl^-/\ SO_4^{2-}$ separation [17–22]. Table 1 summaries the ion characteristics of anions Cl^-, SO_4^{2-} and F^-. Based on the data in Table 1, Cl^- has lower hydration energy, which makes water molecules shedding more easily, allowing the ions to transport through the hydrophobic membrane. In contrast, SO_4^{2-}, with higher hydration energy, binds water clusters firmly, hindering the formation of strong affinity with the functional groups in the membrane. This strategy is promising for separating ions having different hydration behavior. However, if the removal of F^- from SO_4^{2-} is aimed, hydrophobic membranes are no longer suitable, as the strong water-binding capability of F^- restricts its transport ability through the hydrophobic structure [23]. On top of that, SO_4^{2-} is preferentially exchangeable into the AEMs due to its higher valency [24]. Therefore, $F^-/\ SO_4^{2-}$ selectivity is not achieved, which is considered one of the most challenging separation tasks due to the similarity of the hydration ability, migration rate, and transport diameters of respective anions [7].

Another way to influence a membrane's ability to separate ions of the same charge is by introducing ionic groups on the membrane surface having the same sign as the counter-ions [25]. This strategy helps reduce the affinity of multivalent ions with the membrane surface due to the high electrostatic barrier effect and enables the increase of the membrane's top-layer tightness, which restricts the ingress and mobility of bigger ions as a result of the dense layer formation [9,11]. Layer-by-layer (LbL) deposition is a straightforward technique to create an opposite charge and dense layer on the substrate [26]. Several research groups have employed this method on commercial AEMs to investigate monovalent selectivity in a binary mixture [27,28]. Competitive $Cl^-/\ SO_4^{2-}$ selectivity performances were reported, however, a high deposition number of layers was applied (>10). The reason is that the standard AEMs used in these studies generally have high ion exchange capacities (IECs) that lead to the formation of wide hydrophilic entrances and oversized ion channels by the accumulation of solvating water with fixed charge groups in the membrane. When these membranes are modified with fewer layers, the entrance for ions at the surface is not sufficiently covered, thereby still allowing the passage of bigger ions. Hence, more layers are required to reduce the ingress rate of multivalent ions. However, adding more charged layers on a membrane surface tends to increase the surface electrical resistance and instability of the modified layers [29].

Table 1
Ion characteristics of anions.

Anion	Ionic radius (Å) [12]	Hydrated radius (Å) [12]	Charge density ($C{\cdot}mm^{-3}$) [13]	Hydration free energy ($kJ{\cdot}mol^{-1}$) [14]
Cl^-	1.81	3.32	8	- 340
F^-	1.36	3.52	24	- 465
SO_4^{2-}	2.90	3.79	5	- 1080

So far, excellent $Cl^-/\ SO_4^{2-}$ selectivity performances have been reported [20,22,28]. However, the application of reported membranes with superior performance represented is usually limited by either high electrical resistance due to the incorporation of longer alkyl chain length (n > 9) or a high deposition number of polyelectrolyte layers (>10) that causes an impractically long deposition process and increasing the cost of production. Moreover, $F^-/\ SO_4^{2-}$ selectivity through developed AEMs in ED is scarcely reported to the best of our knowledge [7]. Only a few research groups have investigated the separation of F^- from SO_4^{2-}, but merely by using commercial monovalent selective AEMs [2,30–32], and in all these cases, the separation of F^- was only achieved by either using a multiple-stage ED process or with solutions that have high equivalent concentration ratios of SO_4^{2-} and Cl^- to F^- to provide a facilitating F^- transport due to the increased ionic strength effect [2,4]. It is important to note that the removal efficiency of F^- is not satisfactory for the equimolar solutions, where its removal should be mainly decided by the IEM properties rather than process conditions. Therefore, efforts to design IEM of desired properties for F^- removal from SO_4^{2-} is significantly required.

This study aims to develop novel monovalent selective AEMs due to inspiration from an urgent need for the challenging separation of F^- from SO_4^{2-} and its simultaneous removal with Cl^- in an equimolar ternary mixture to meet industrial demands. We have optimized the design of both the matrix and surface of the AEMs to improve the target ions' (Cl^- and F^-) permeability through the membranes. Brominated poly(2,6-dimethyl-1,4-phenylene oxide) (BPPO) polymers were synthesized at different reaction temperatures, which determined the selectivity of bromination to the benzyl or aryl positions. Quaternization was performed using two different tertiary amines with varied chain lengths for further optimization of the membrane microstructure. The mobility and interaction of the ions with the fixed groups in the membrane matrix were found to be significantly affected by the polymer structure design. Using the optimized matrix as the substrate also reduced the required number of deposition layers for the simplicity and economics of the process. Surface modification was applied to reduce the affinity and ingress rate of divalent anions at the membrane interface. To test our hypothesis, unmodified and modified AEMs were analyzed with an equimolar mixture of Cl^-, F^-, and SO_4^{2-}. Monovalent selective commercial ASVN was also tested for comparison. To the best of the authors' knowledge, this study is the first to present the design of AEMs for the simultaneous separation of Cl^- and F^- from SO_4^{2-} in an equimolar ternary mixture using ED.

2. Materials and methods

2.1. Materials

PPO (M_n = 20,000 g mol^{-1}, M_w = 30,000 g mol^{-1}, Aldrich), 2,2′-Azobisisobutyronitrile (AIBN, 98%, Aldrich), N-bromosuccinimide (NBS, 99%, Aldrich), chlorobenzene (99.5%, Aldrich), chloroform (99.5%, Aldrich), ethanol (100%, VWR), trimethylamine (TMA, 45 wt% aqueous solution, Aldrich), dimethylhexylamine (DMHA, 98%, Aldrich), N-methyl-2-pyrrolidone (NMP, 99.5%, Aldrich), deuterated chloroform ($CDCl_3$, 99%, Aldrich) and dimethyl sulfoxide (DMSO-d_6, 99.8%, Aldrich) were used as received. Silver nitrate ($AgNO_3$, 99%, Aldrich) and TISAB solution (Supelco) were used to determine Cl^- and F^- concentrations, respectively. Poly (sodium 4-styrenesulfonate) (PSS) (M_w = 70,000 kDa, Aldrich) and poly(allylamine hydrochloride) (PAH) (M_w = 17,500 Da, Aldrich) were used as anionic and cationic polyelectrolyte layers. Sodium hydroxide (NaOH, Aldrich) and hydrochloric acid (HCl, Aldrich) were used to adjust the pH of polyelectrolyte solutions. To test the selectivity performance, sodium chloride (NaCl, Aldrich), sodium fluoride (NaF, Aldrich) and sodium sulfate (Na_2SO_4) were used as the

source of monovalent and divalent anions. PC MTE (end-CEM, PCCell GmbH, Germany) and ASVN (AEM, Selemion, Japan) were also used in ED tests.

2.2. Bromination of PPO

PPO was brominated via a slight adjustment based on the method reported in the literature [33]. The procedure was described as follows (Scheme 1a): 6 g (50 mmol) of PPO was slowly added to 100 mL of chlorobenzene in a 250 mL round bottom three-neck flask equipped with a water-cooling condenser. The mixture was magnetically stirred continuously until complete dissolution was achieved at room temperature. 4.45 g (25 mmol) NBS and AIBN (3 mol% to the amount of PPO dissolved), a free radical initiator, were added to start the reaction. Subsequently, the mixture was subjected to the bromination reaction at the desired temperature for 3 h in an oil bath. The temperature was altered to control the selective reaction of bromine to the benzyl or aryl positions. During the reaction, the color of the solution turned dark brown at higher temperatures and red at lower temperatures. An argon purge was used to remove hydrogen bromide gas formed during the reaction, which was absorbed in 10 wt% NaOH solution. After the reaction, the temperature was decreased to room temperature. The reaction mixture was slowly poured into mechanically stirred 1000 mL of ethanol to precipitate polymers and remove residual chlorobenzene. Then, the polymers were recovered by filtration and dried overnight. Dried polymers were dissolved in 70 mL of chloroform for further purification and then precipitated with ethanol to give the pure product. The recovered polymers were washed many times with ethanol to remove the residual solvent, followed by drying in a vacuum oven at 80 °C for 24 h.

2.3. Preparation of bare AEMs with quaternization of BPPO

1.7 g BPPO was dissolved in NMP to generate a homogeneous solution with a concentration of 15% (w/w). Then, TMA or DMHA with a mole ratio of 2:1 to the amount of the benzyl brominated part of the polymer was added. Quaternization only occurred with benzyl-substitution groups (Scheme 1b) [34]. The reaction mixture was continuously stirred for 48 h at room temperature. Finally, the mixture was cast onto a clean glass plate using a steel knife with a wet thickness of 700 μm, followed by solvent evaporation at 60 °C for 24 h under a vacuum. After soaking in deionized water, the resulting AEMs were peeled off from the glass plate and stored in the refrigerator. Bare AEMs were named QPPOx_y, where x denotes the bromination reaction temperature and y corresponds to the quaternary agent (Table 2).

2.4. Surface modification of bare AEMs

LbL deposition was performed with PSS polyanion in 0.5 M NaCl and PAH polycation in 1.0 M NaCl (Scheme 2a). Bare AEMs were kept in a holder to restrict the film forming on only one side of the membrane. The pH and concentration of polyelectrolyte solutions were adjusted to 2.3 and 0.02 M of the polymer repeating unit, respectively. LbL was initiated with PSS deposition on bare AEM (Scheme 2b). After each deposition, the membrane surface was rinsed with deionized water for ~60 s to remove excess and weakly adsorbed polyelectrolytes. LbL deposition took 10 min for each layer except for the first layer, which contacted the membrane surface for 30 min. Modified AEMs were named QPPOx_y_$(PSS/PAH)_n$, where n represents the number of layers (i.e., n = 2.5 means 5 layers in total, 3 layers of PSS and 2 layers of PAH).

2.5. Characterization and measurements

2.5.1. ^1H nuclear magnetic resonance and Fourier transform infrared spectroscopy

^1H nuclear magnetic resonance (^1H NMR) and Fourier transform infrared spectroscopy (FT-IR) spectra were employed to characterize the chemical structure of PPO and BPPO polymers and bare AEMs. ^1H NMR spectra were recorded with a Bruker Avance 600 Neo spectrometer at 600 MHz using deuterated $CDCl_3$ solvent for brominated polymers and DMSO-d_6 solvent for bare AEMs. The degree of bromination (DB) on aryl and benzyl positions was calculated under the areas of these peaks using equations (1) and (2) [35]:

$$DB_{Br\ to\ aryl} = \frac{Area\ peak\ at\ (6.0-6.4)}{Area\ peak\ at\ (6.4-7.0) + 2 \cdot Area\ peak\ at\ (6.0-6.4)} \quad (1)$$

Table 2
Synthesized bare AEMs from BPPO polymers and tertiary amines.

Bromination temperature (°C)	Polymer backbone	Tertiary amine (alkyl chain length, n)	Bare AEM after quaternization
60	BPPO60	DMHA (n = 6)	QPPO60_DMHA
60	BPPO60	TMA (n = 1)	QPPO60_TMA
85	BPPO85	TMA (n = 1)	QPPO85_TMA
135	BPPO135	TMA (n = 1)	QPPO135_TMA

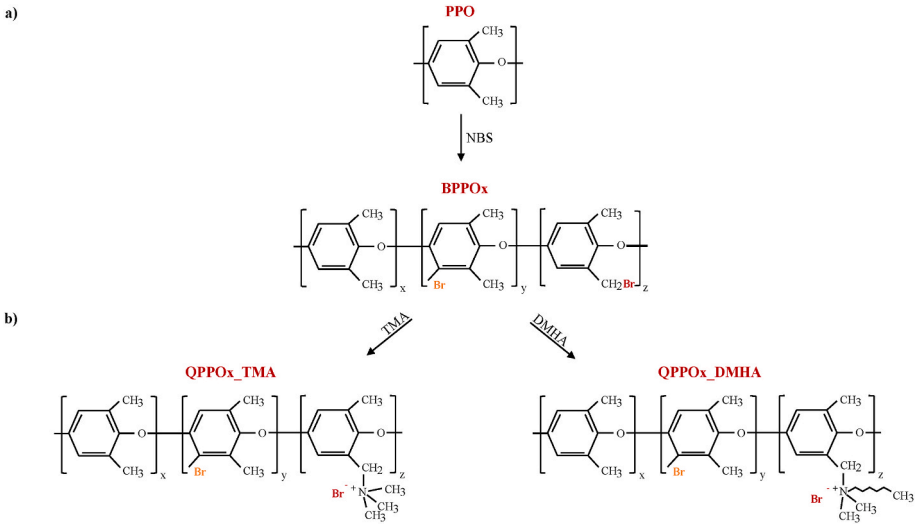

Scheme 1. Preparation route of bare AEMs; a) bromination of PPO in aryl and benzyl positions; b) quaternization of BPPO with TMA or DMHA.

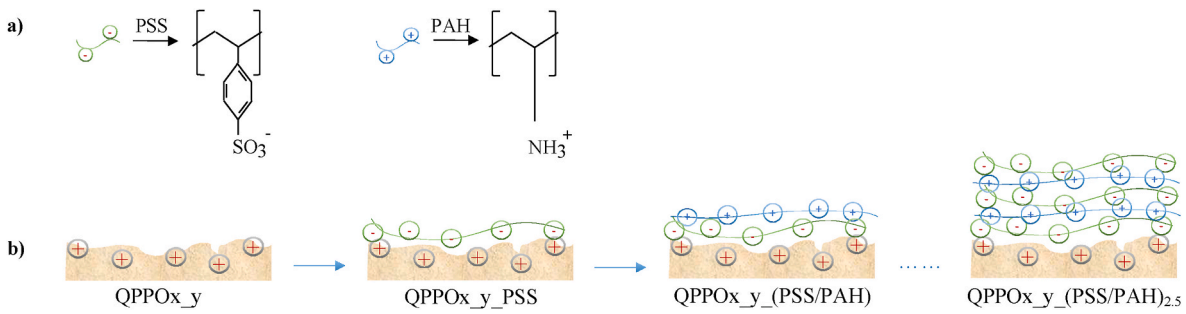

Scheme 2. a) Polyelectrolytes used in the LbL deposition; b) alternating polyelectrolyte assembly on bare AEM.

$$DB_{Br\ to\ benzyl} = \frac{Area\ peak\ at\ 4.3}{Area\ peak\ at\ (6.4-7.0) + 2{\cdot}Area\ peak\ at\ (6.0-6.4)} \quad (2)$$

The FT-IR spectra (iS50 FT-IR, Thermo Scientific) of BPPO polymers and bare AEMs were recorded (1000–4000 cm^{-1}).

2.5.2. Ion exchange capacity, water uptake, swelling ratio, fixed charge concentration, and hydration number

IEC of bare AEMs was determined by potentiometric titration (Mettler Toledo, Easy Cl). A piece of membrane in Br^- form was dried in an oven under a vacuum at 60 °C. After drying, membrane samples were weighed and immersed in 1.0 M NaCl aqueous solution for 24 h to exchange Br^- with Cl^-. AEMs were rinsed with deionized water to remove the excess Cl^-. Then, the pieces of the membrane were soaked in 0.5 M Na_2SO_4 aqueous solution for another 24 h to release Cl^- anions from AEM samples by exchanging with SO_4^{2-}. 0.1 M $AgNO_3$ was used to titrate the solution, including exchanged Cl^- from AEM samples. The IEC values were calculated according to equation (3) [36]:

$$IEC\left(\frac{mmol}{g}\right) = \frac{V_{Na_2SO_4}{\cdot}C_{Cl^-}}{m} \quad (3)$$

where V is the volume of Na_2SO_4 solution (L) used for immersing membrane samples containing Cl^-, C_{Cl^-} is the concentration of Cl^- (M) titrated by $AgNO_3$ solution, and m is the dry weight of membrane samples (g).

Water uptake (WU) and swelling ratio (SR) were determined by the difference in weight and dimension of dry and wet membrane samples. First, membrane samples were cut into 1 cm × 4 cm and dried in an oven at 60 °C under a vacuum for 24 h. Then, the weight and length of the dried samples were measured. Subsequently, the samples immersed in deionized water for 24 h at room temperature. The weight and dimension of the wet samples were measured right after removing the excess surface water. WU and SR values were calculated according to equations (4) and (5) [36]:

$$WU\ (\%) = \frac{(W_{wet} - W_{dry})}{W_{dry}}{\cdot}100\% \quad (4)$$

$$SR\ (\%) = \frac{(l_{wet} - l_{dry})}{l_{dry}}{\cdot}100\% \quad (5)$$

where W_w and W_d represent the mass of the wet and dry membrane samples, respectively; l_w and l_d are the lengths of the wet and dry membrane samples, respectively. The IEC and WU can be used to determine the membrane fixed charge concentration (FCC) and hydration number (λ) from equations (6) and (7) [37]:

$$FCC\left(\frac{mol}{L}\right) = \frac{IEC}{WU}{\cdot}\rho_w \quad (6)$$

$$\lambda = \frac{WU{\cdot}1000}{IEC{\cdot}M_w} \quad (7)$$

where ρ_w and M_w are the density and molecular weight of water, respectively.

2.5.3. Electroosmotic water transfer

Electroosmotic water transfer (EWT) of the AEMs was also measured by the Micro BED System, comprises of a coulomb counting device that automatically applies a 120 A · s package of charge for a given volume. Fig. 1 shows the schematical setup of the EWT measurement. The applied current was 0.3 A during the operation. The electrode chamber was circulated with 0.25 M Na_2SO_4 rinse solution, while diluate chamber was fed with 1 M NaCl solution. The open chamber was used as a concentrate chamber and filled with 1 M NaCl without circulation. The investigated AEM was placed between the end-CEM and hydrophobic CEM (PC S 100, PCCell GmbH). End-CEMs and hydrophobic CEM were used to limit the interference of the electrolyte solutions and water transport, respectively. A certain amount of water is transferred through the AEM from the diluate chamber into the concentrate chamber by applying a current. The volume increase in the concentrate chamber was quantified via a pipette. The EWT was calculated from equation (8):

$$\mathrm{EWT}\left(\frac{mol\ H_2O}{mol\ e^-}\right) = \frac{\mathrm{dn_w}}{\mathrm{Q}{\cdot}F^{-1}} = d\left(\frac{\rho_w{\cdot}V_w}{M_w}\right){\cdot}\frac{\mathrm{F}}{I{\cdot}dt} \quad (8)$$

where n_w, V_w, ρ_w, and M_w are mole, volume (mL), density (g · mL^{-1}), and molecular weight (g · mol^{-1}) of water, Q is the quantity of charge transported (Coulomb), F is Faraday constant (96,485.3 C · mol^{-1} e^-), I is applied current (C · s^{-1}), and dt (s) is the time change.

2.5.4. Water contact angle

Water contact angle measurements were performed by an optical tensiometer (T330, Biolin Scientific) to determine the surface hydrophobicity of membranes. Moreover, it was used to monitor the deposition of the polyelectrolyte layers. The membranes were dried and fixed on a glass slide before the measurement. Four measurements were performed for each membrane with 4 μl deionized water droplets.

2.5.5. Scanning electron microscopy

The surface topography of unmodified and modified AEMs was characterized by a field emission scanning electron microscopey (FESEM) (Apreo, FEI). The SEM samples were cut into small pieces and dried under vacuum at 25 °C before the analysis. Then, the samples were fixed on an SEM sample holder with single-sided copper tape.

2.5.6. X-ray photoelectron spectroscopy

XPS was mainly used to determine the surface elemental composition of bare AEMs and confirm the deposited polyelectrolyte layers (Axis Ultra DLD, Kratos Analytical).

2.5.7. Monovalent anion selectivity measurements

Monovalent selectivity measurements were performed by a standard ED device supplied by PCCell Micro BED System. The membrane stack consists of four chambers with one diluate, one concentrate, and two

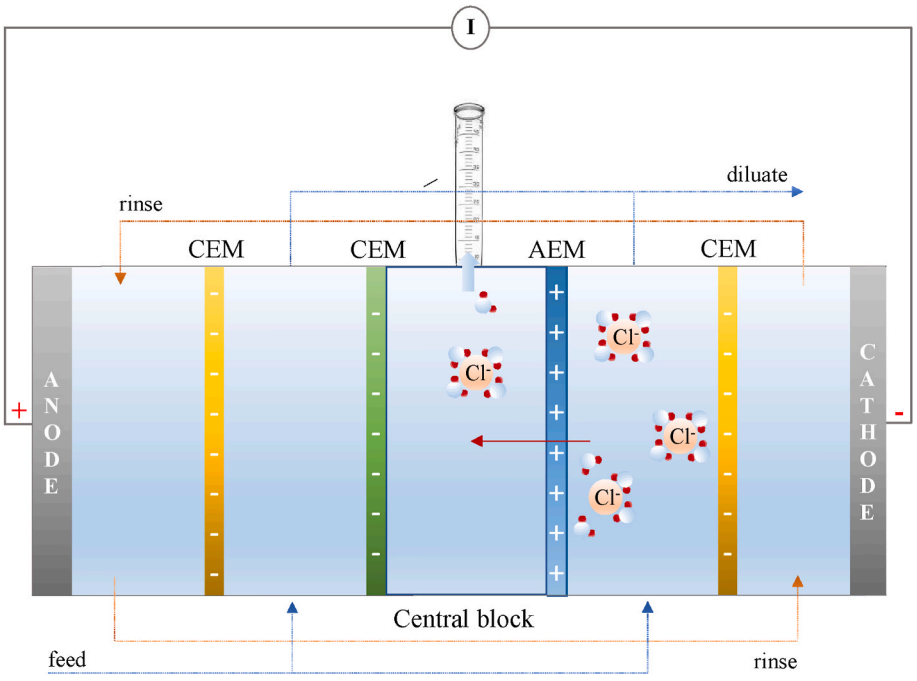

Fig. 1. Schematic representation of EWT measurement. Yellow membranes denote for end-CEMs while the green one corresponds to the hydrophobic CEM. (For interpretation of the references to color in this figure legend, the reader is referred to the Web version of this article.)

electrode chambers (Fig. 2). Developed AEMs were placed in the middle of the cell to investigate the transfer of anions from diluate to concentrate chambers. Commercial end-CEMs were used at both ends of the stack to restrict the interference of the electrolyte solutions during the operation of ED. The membranes have an effective area of 6 cm^2. Electrode chambers were circulated with 90 mL 0.25 M Na_2SO_4 electrolyte solution, while concentrate and diluate chambers were fed with 175 mL 10 mM mixture of NaCl, NaF and Na_2SO_4. The circular flow rate was kept constant for diluate and concentrate chambers which were set at 120 mL/min 10 mA cm^{-2} current density was generated during the operation. The measurement lasted for 60 min at room temperature. Samples were collected from both chambers at regular intervals to determine the ions' concentrations. Cl^-, F^-, and SO_4^{2-} content in the samples were determined by Easy Cl (Mettler Toledo), pH/ION 7320 (inoLab) and ion chromatography (Metrohm 940 Professional IC Vario 1, Switzerland), respectively.

The ion selectivity $[P_B^A]$ of the membranes was obtained from equation (9) [38]:

$$P_B^A = \frac{\frac{t_A}{t_B}}{\frac{C_A}{C_B}} = \frac{J_A \cdot C_B}{J_B \cdot C_A} \tag{9}$$

where t_A and t_B are the transport number (dimensionless) of components A and B in the membrane phase, C_A and C_B (mol·L^{-1}) are the average concentrations on the diluate side of the membranes, J_A and J_B (mol·m^{-2}·s^{-1}) are the flux of the components A and B. Ion flux was given by equation (10) [38]:

$$J_A = \frac{V \cdot \frac{dC_i}{dt}}{A} \tag{10}$$

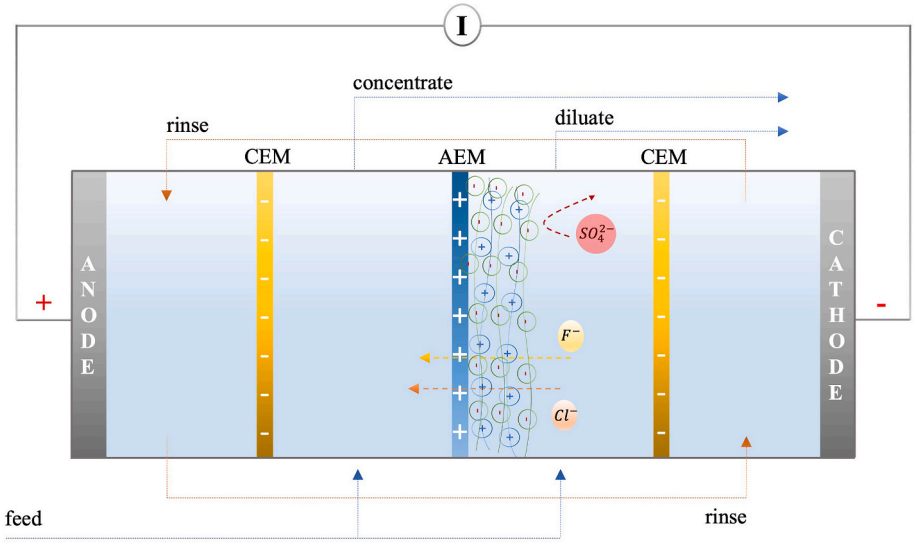

Fig. 2. Membrane stack assembly in ED cell.

where V (L) is the volume of solution, dC_i (mol·L^{-1}) is the concentration change of the component i on the diluate side at time t, dt (s) is the time change, and A (m^2) is the active area of the membrane. Moreover, energy consumption (E_m) in the membrane region was calculated according to equation (11) [38]:

$$E_m = \frac{\int U_m \cdot I \cdot dt}{(C_0 - C_t) \cdot V} \quad (11)$$

where U_m is the voltage drop across the membrane, I is the applied current, dt (s) is the time change, and C_0 and C_t are the concentrations of Cl^- or F^- ions initially and at a specific time t. The Gibbs free energy of mixing was also calculated to demonstrate the minimum energy required for the separation of anions during ED operation [39]. The derivation of the general expression of the Gibbs free energy of mixing is given as Supporting Information.

3. Results and discussion

3.1. ^{1}H nuclear magnetic resonance and Fourier transform infrared spectroscopy

The ^{1}H NMR spectra of the PPO, BPPO and bare AEMs are shown in Figs. S1a and b. Successful bromination in the benzyl and aryl groups of the polymer was confirmed by the proton peaks at 4.3 ppm and 6.2 ppm (Fig. S1a) [35]. The area of peaks at 4.3 ppm and 6.2 ppm altered depending on the bromination reaction temperature. As the reaction temperature increased, protons in the methyl group adjacent to the bromine resulted in higher peaks. When the bromination was conducted at 135 °C, the proton peaks at the aryl position (6.2 ppm) completely disappeared, and the area under benzylic proton peaks reached its maximum value. Reciprocally, lowering the bromination reaction temperature favored the formation of higher bromine peaks at the polymer's aromatic backbone. Nevertheless, total bromination was conserved regardless of the reaction temperature because the amount of NBS was kept constant (Table 3). The ^{1}H NMR spectra of the successful incorporation of tertiary amines (TMA or DMHA) was also confirmed by the appearance of new peaks. The ^{1}H NMR peak of the bromobenzylic proton at 4.3 ppm disappeared, and new benzylic proton peaks next to the head group of tertiary amines appeared at 3.1 ppm (Fig. S1b) [35]. Based on the characteristic peaks from ^{1}H NMR, it can be concluded that tertiary amines were successfully grafted onto the BPPO backbones.

The FT-IR spectra of PPO, BPPO and AEMs were also investigated to confirm the quaternization reaction between carbon in the methyl group adjacent to the bromine and nitrogen in the head groups of tertiary amines (Fig. 3). The peaks positioned approximately at 1185 cm^{-1}, 1305 cm^{-1}, 1469 cm^{-1}, and 1602 cm^{-1} were related to the PPO polymer [40]. The intensity peaks at 1185 cm^{-1} and 1602 cm^{-1} were attributed to the stretching vibrations of C–O–C and C═C. On the other hand, the band at ~1730 cm^{-1} was attributed to the C–N bond vibration of the quaternary ammonium groups [41]. Notably, this band was generated in the spectrum of neither PPO nor BPPO polymer. An additional broad peak appeared at 3400 cm^{-1} assigned to the vibration of the O–H bond owing to the existence of hydrophilic hydrated amine groups in QPPO [41].

Table 3
Bromination degree of PPO polymers at the different reaction temperatures.

Reaction temperature (°C)	Degree of bromination in benzyl position (%)	Degree of bromination in aryl position (%)	Total bromination (%)
60	8.4 ± 0.3	18.3 ± 0.2	26.2 ± 0.2
85	19.5 ± 0.2	6.7 ± 0.2	26.7 ± 0.3
135	26.8 ± 0.3	0	26.8 ± 0.3

3.2. Ion exchange capacity, water uptake, swelling ratio, fixed charge concentration, and hydration number

The IEC is a measure of the number of fixed charges per unit mass of dry polymer of the membrane, which provides insight into the concentration of free charge [42]. It is a crucial membrane property influencing ions' transport rate. As shown in Table 4, IECs range from 0.84 ± 0.02 mmol·g^{-1} to 1.84 ± 0.03 mmol g^{-1} for developed membranes. AEMs displayed higher IECs as the bromination degree increased in the polymer's benzyl position, which indicated the quaternization of tertiary amines occurred only with carbon adjacent to the bromine in the benzyl substitution group. Therefore, membranes prepared from polymers brominated at 135 °C offered the highest IEC. On the contrary, IECs decreased for the membranes possessing higher bromination degree in the aryl position as aryl-substitution groups could not react with tertiary amines. Noticeably, when TMA was replaced with DMHA, the IEC kept almost constant, while WU and SR decreased for BPPO60-based membranes. It can be explained that a tertiary amine with a longer alkyl chain length suppressed the water adsorption while providing almost the same quaternization capability due to having the same amount of bromine in BPPO60.

A membrane possessing high IEC tends to take up a large amount of water when immersed in aqueous solutions. This, in turn, results in higher swelling capacity for the membrane due to the hydration of ion exchange groups, which explains why QPPO135_TMA represented the highest WU and SR among all developed membranes. On the other hand, AEMs with a higher degree of bromination in the aryl substitution position represented lower WU and SR due to less tertiary amine incorporation, thereby less contribution to the IEC, WU, and SR. Another reason for displaying a more hydrophobic character of the membranes was due to the high bromine content in the aryl group that increased the rigidity of the polymer [43]. Furthermore, the length of the alkyl chain is also decisive in adjusting the hydrophobicity of the membranes, from which the hydrophilic-lipophilic balance can be interpreted. The hydrophilic–lipophilic balance value of TMA (14.98) was reported as less than that of DMHA (12.63) [18]. Further decrease in WU and SR values from QPPO60_TMA to QPPO60_DMHA agreed with the effect of this balance. Notably, the ASVN membrane represented lower SR despite having higher IEC than the QPPO80_TMA and QPPO135_TMA membranes due to the reinforcement of the membrane causing swelling only in one direction [44].

According to the solution-diffusion model, ion sorption and mobility are the main steps for ion transport through a dense, nonporous membrane [45]. Ion sorption in charged polymers is usually governed by the concentration of fixed charge groups (fixed charge groups per volume of imbedded water) and the polymer's water content (the number of bonded water per fixed group). Therefore, counter-ion selectivity can be dominated by the distribution and concentration of the fixed charge groups and their bonding water inside the IEMs [37]. Herein, FCC and λ of the developed AEMs are represented in Table 4. FCCs displayed the opposite trend compared to the IEC and WU of the AEMs. For instance, the FCC of QPPO60_TMA was almost twice as much as of QPPO135_TMA. Moreover, when DMHA was incorporated instead of TMA, FCC reached its maximum value despite their similar IECs. That is the critical indication of developing membranes with higher FCCs by keeping their IECs constant while improving hydrophobic character. On the contrary, λ values compromised the IEC and WU of the membranes and changed proportionally with the hydrophobicity of the membranes. It is essential to keep λ values at low levels, which confirms the anti-swelling property and affects the dimensional stability of the membranes, influencing ion selectivity [36].

3.3. Electroosmotic water transfer

In most cases, water transport by osmosis can be neglected in the presence of an applied electric current [48]. That is, osmosis is still

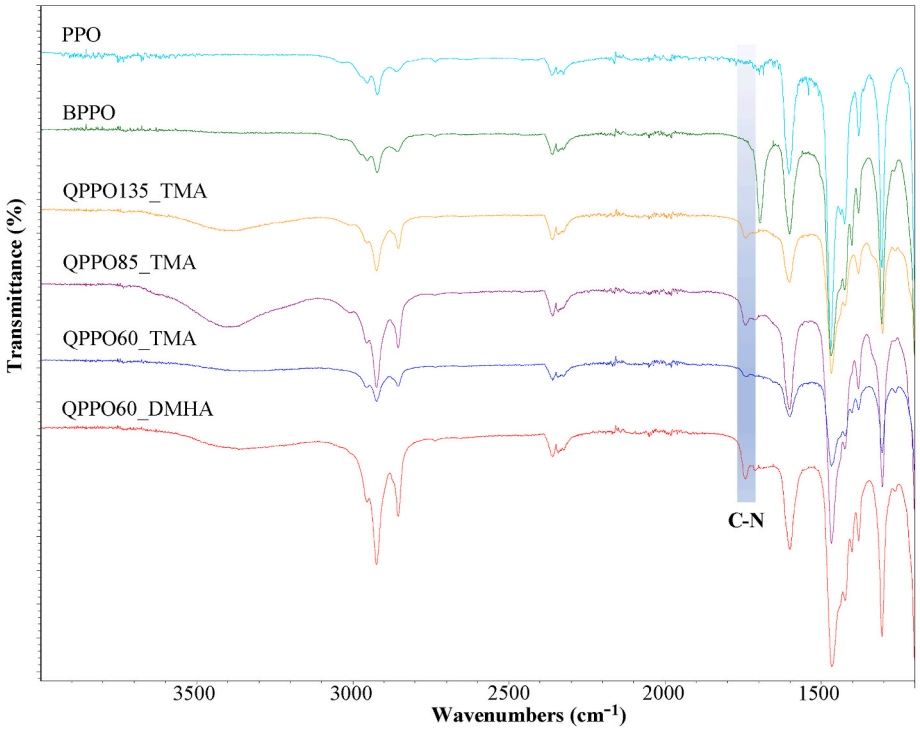

Fig. 3. FT-IR spectra of PPO, BPPO polymers, and AEMs.

Table 4
Physicochemical properties of the AEMs.

AEM	Thickness (μm)	IEC (mmol·g^{-1})	WU (%)	SR (%)	FCC (mol·L^{-1})	λ
QPPO60_DMHA	86 ± 1.4	0.84 ± 0.02	4.6 ± 0.2	1.3 ± 0.01	18.2 ± 0.2	3.1 ± 0.2
QPPO60_TMA	86 ± 0.9	0.89 ± 0.01	6.9 ± 0.2	2.7 ± 0.03	12.9 ± 0.3	4.3 ± 0.3
QPPO85_TMA	86 ± 0.7	1.54 ± 0.02	19.0 ± 0.04	6.3 ± 0.5	8.1 ± 0.1	6.9 ± 0.1
QPPO135_TMA	86 ± 1.2	1.84 ± 0.03	27.6 ± 0.2	8.7 ± 0.1	6.7 ± 0.3	8.3 ± 0.3
ASVN	120 ± 0.5	1.99 ± 0.01	20.5 ± 0.2	7.5 ± 0.2	9.7 ± 0.4	5.7 ± 0.5

present when a current is applied, but the co-transport of water far exceeds the flux by osmosis. As such, we attribute the water crossover to be caused by co-transport in this study. Water is polarizable, and when salts are dissolved, a hydration shell is formed around the ions [11]. Hence, ion transport in solution is correlated with the radius of hydrated ions rather than simply the radius of the bare ion. A good ED process intends to move the ions without water molecules, which can cause a decrease in the process performance, but water transport is, to some extent, inevitable [46]. Consequently, it is a virtual point of interest to determine how much water moves with one ion in the ED process. During the transport of ions, water transfer can be carried out either by electro-osmosis co-transport or by osmosis [47].

EWTs of AEMs are displayed in Fig. 4. The amount of water transported varied for different membranes due to differences in membranes' water content [47]. The least amount of water molecules (4.57 ± 0.53) transferred through the QPPO60_DMHA membrane owing to the

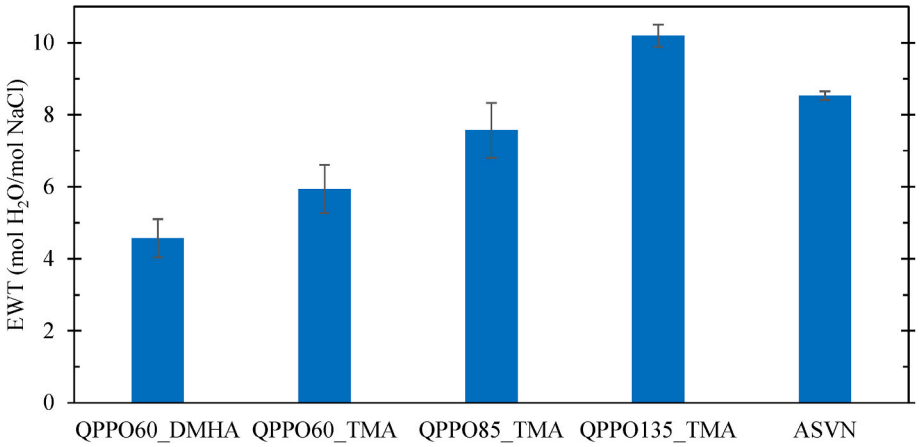

Fig. 4. EWT of bare and commercial AEMs.

presence of the long alkyl chain length having less ability to hold water molecules. It is also important to note that the anti-swelling property of the membrane leads to narrow ionic aqueous domains in the network and lower water transport [49]. Moreover, weakly hydrated Cl^- is susceptible to shed water molecules from their hydration shells due to its lower hydration free energy when encountering hydrophobic domains in the membrane. Therefore, the number of water molecules accompanied by Cl^- anions decreases with an increase of hydrophobic property of the membrane. This indicated that the membrane network having a more hydrophobic structure suppressed the water migration most. On the other hand, since water permeability tends to be closely related to water sorption, a higher amount of fixed charged groups on the polymer chain resulted in higher WU and SR of the membranes, which caused the water transfer of the membranes to increase [50]. EWTs of QPPO85_TMA, ASVN, and QPPO135_TMA AEMs were found 7.57 ± 0.76, 8.53 ± 0.12, and 10.19 ± 0.31, respectively. Even though the ASVN membrane had the highest IEC, its water transport was less than QPPO135_TMA due to less WU and SR of the membrane.

3.4. Water contact angle

In order to evaluate the surface hydrophobicity and confirm the deposition of polyelectrolyte layers, water contact angle measurements of bare and LbL-modified AEMs were performed. The water contact angles were found 93.7 ± 2.1°, 85.7 ± 1.2°, 79.4 ± 0.9°, 73 ± 1.3°, and 56.2 ± 1.9° for QPPO60_DMHA, QPPO60_TMA, QPPO85_TMA, QPPO135_TMA, and ASVN, respectively (Fig. 5). As the bromination degree of PPO increased in aryl positions, the quaternization capacity of the polymer backbone with tertiary amines was restricted. Moreover, incorporating the hydrophobic side chains of DMHA into the polymer backbone yielded a higher hydrophobic atmosphere in the AEM matrix. These structures prevented the backbone from holding water, retaining a low SR and high water contact angle. On the other hand, membranes with higher IECs could take up a large amount of water, presenting lower water contact angles.

Water contact angles of the LbL-modified membranes are also investigated. For all membranes, the water contact angle decreased after modification. This decrease can be ascribed to the termination of the last layer with PSS polyelectrolyte, providing sulfonic groups that can be easily hydrated. This phenomenon indicated that multilayer membranes became more hydrophilic after the polyelectrolyte deposition. Noticeably, water contact angles were found different after the deposition since the amount of adsorption was different for each membrane.

3.5. Scanning electron microscopy

To further verify the deposition of PSS and PAH layers, membrane surface morphology was analyzed by FESEM. Fig. 6 shows surface topography images of the QPPO85_TMA membrane and its coated form with a $(PSS/PAH)_{2.5}$ film with same the magnification. The surface of modified membranes was also displayed with higher magnification. The bare membrane demonstrated a smooth surface. After deposition, the small nodules of polyelectrolyte complexes were observed, suggesting the successful deposition on the membrane surface.

3.6. X-ray photoelectron spectroscopy

Fig. 7 represents the ratio of atomic concentration between nitrogen (N) associated with PAH and sulfur (S) corresponding to the PSS. When the number of deposited layers was an even number, the N/S ratio increased due to the termination of the last layer with PAH possessing amine groups. Reciprocally, the N/S ratio decreased for odd numbers due to the contribution of the sulfur content from PSS. Therefore, the alternating increase and decrease trends proved the successful coating procedure after each layer. When the deposition number of layers is low, XPS can be used as an effective method to validate the presence of deposited layers [38].

Table 5 presents the total increase of N% and S% for the modified membranes. The elemental increase of N% was found to be the lowest for the QPPO60_DMHA and QPPO60_TMA membranes. On the contrary, the N% increase was most pronounced for the QPPO85_TMA and QPPO135_TMA membranes. It can be attributed to the high IEC values of the QPPO85_TMA and QPPO135_TMA membranes providing higher adsorption capacity for polyelectrolyte segments. The same trend was also observed for the S% increase, which was in the increasing order of IEC values of the bare membranes. Furthermore, the sharp increase and decrease trends of N/S were displayed for QPPO85_TMA and QPPO135_TMA, while the trends were less dramatic for QPPO60_DMHA and QPPO60_TMA, compromising the extent of adsorption on the membranes.

3.7. Monovalent anion separation performance

ED tests were carried out to investigate the monovalent selectivity performances of developed membranes. Four kinds of bare AEMs with different microstructures were synthesized to explore their effect on the permeation ability of ions. Subsequently, AEMs were modified with polyelectrolyte layers to enhance monovalent selectivity by Donnan and size exclusion mechanisms [49,51]. The ASVN membrane was also

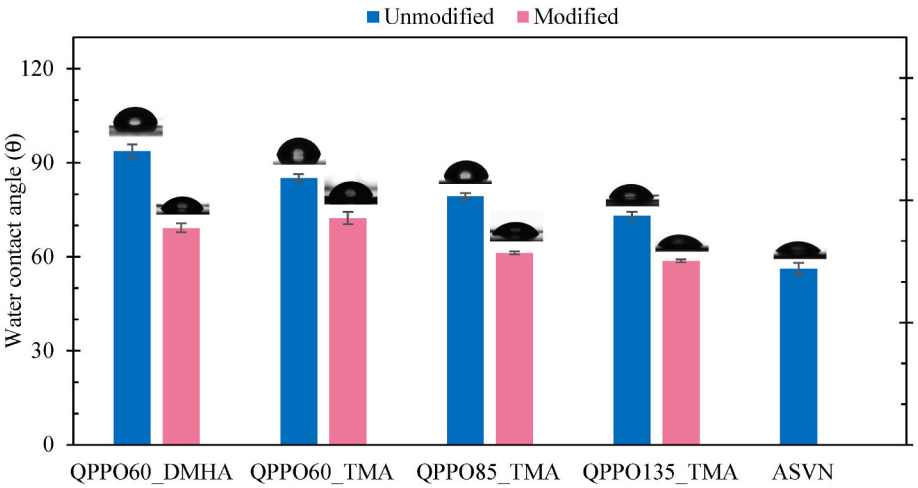

Fig. 5. Water contact angles of bare, modified, and commercial AEMs.

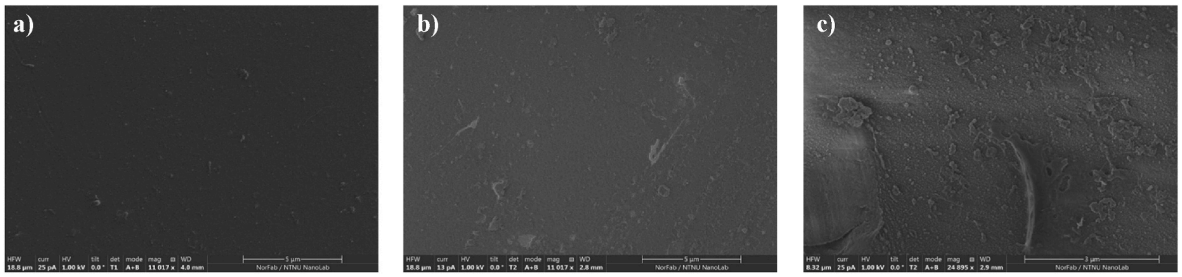

Fig. 6. FESEM images of (a) bare QPPO85_TMA membrane; (b) bare QPPO85_TMA membrane modified with 5 layers of PSS/PAH; (c) bare QPPO85_TMA membrane modified with 5 layers of PSS/PAH with higher magnification.

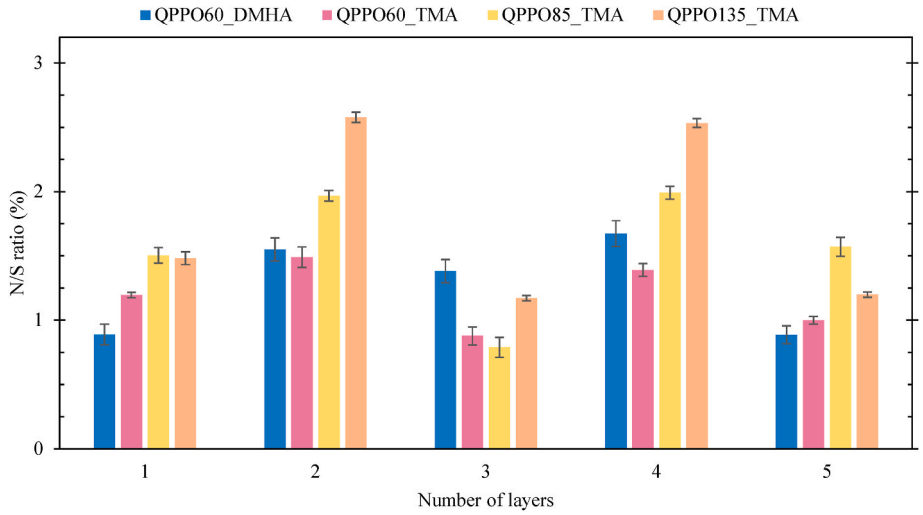

Fig. 7. N/S ratio of LbL-modified AEMs for each deposition layer.

Table 5
Percent increase of N and S elements on bare AEMs.

Unmodified AEM	N % increase (from bare to 4th layer)	S % increase (from 1st to 5th layer)
QPPO60_DMHA	1.05 ± 0.09	1.97 ± 0.15
QPPO60_TMA	1.03 ± 0.12	2.06 ± 0.03
QPPO85_TMA	1.90 ± 0.05	2.32 ± 0.09
QPPO135_TMA	2.15 ± 0.07	2.40 ± 0.02

tested for comparison. Flux and monovalent selectivity performances of all resulting membranes are depicted in Fig. 8. The concentration profiles of anions used to calculate flux and selectivity performances are represented as Supporting Information (Figs. S2–S10). Results indicated that anions transferred through developed membranes at different rates.

As it can be seen from Fig. 8a, the flux of SO_4^{2-} (22.5 ± 0.28 nmol cm^{-2} s^{-1}) was much higher than that of F^- (7.9 ± 0.58 nmol cm^{-2} s^{-1}) and slightly higher compared to Cl^- (20.9 ± 0.55 nmol cm^{-2} s^{-1}) for the QPPO135_TMA membrane. Higher valency prioritized the preferential exchange of SO_4^{2-} with fixed positive charged groups in the membrane due to a stronger electrostatic attraction force. Furthermore, too many hydrophilic fixed groups led to high SR increasing the hydrophilic entrances and water channels of the membrane, thereby accelerating the ingress and migration rates of bigger ions [50]. On the other hand, when the valency of ions is equal (i.e., Cl^- and F^-), their permeation order is mainly determined by the strength of coordination of water molecules around ions affecting their Coulombic interaction with the fixed ionic groups in the membrane [52]. Cl^- has a lower charge density than F^- due to its bigger ionic radius (Table 1) [13]. Hence, Cl^- binds water clusters weaker than F^-, which implies that Cl^- can establish a closer approach to the positively charged fixed groups. It was also previously reported that F^- has a lower ion exchange equilibrium constant with TMA than Cl^- [23]. All of the above-mentioned caused ion permeation in the order of $SO_4^{2-} > Cl^- > F^-$ (Scheme 3a). Therefore, monovalent selectivity was not achieved through the QPPO135_TMA membrane (Fig. 8c).

When the IEC of the membranes decreased with more aryl bromination on the polymer network, an apparent increase in flux values was observed for both monovalent anions, whereas the flux of divalent anions decreased (Fig. 8a). This trend is resulted from the decrease of hydrophilic precursors, causing fewer water channels and less SR, and the rigidity increase after aryl bromination, leading to a denser structure in the membrane network [20,43]. These, in turn, reduced the entrance and mobility of bigger ions through the membranes. Therefore, Cl^-/SO_4^{2-} and F^-/SO_4^{2-} selectivities were enhanced for QPPO85_TMA and QPPO60_TMA compared to QPPO135_TMA. However, the incorporation of tertiary amine of higher chain length into the membrane network (QPPO60_DMHA) caused F^-/SO_4^{2-} selectivity to decrease while Cl^-/SO_4^{2-} selectivity performance kept increasing (Fig. 8c). This can be attributed to the differences in ions' hydration energy, the energy barrier that an ion must overcome to pass the membrane interface. While Cl^- anions can rearrange the hydration shells and lose water molecules, SO_4^{2-} anions hardly remove the hydration shells during their transport through the hydrophobic membrane (Table 1). In this case, the dehydration-based energy barrier suppresses the electrostatic attraction-based affinity of SO_4^{2-}, which caused Cl^- anions to get closer than SO_4^{2-} to the surface of the QPPO60_DMHA membrane. Another reason for a distinguished Cl^-/SO_4^{2-} performance was the anti-swelling property (λ) and denser network of QPPO60_DMHA restricting the

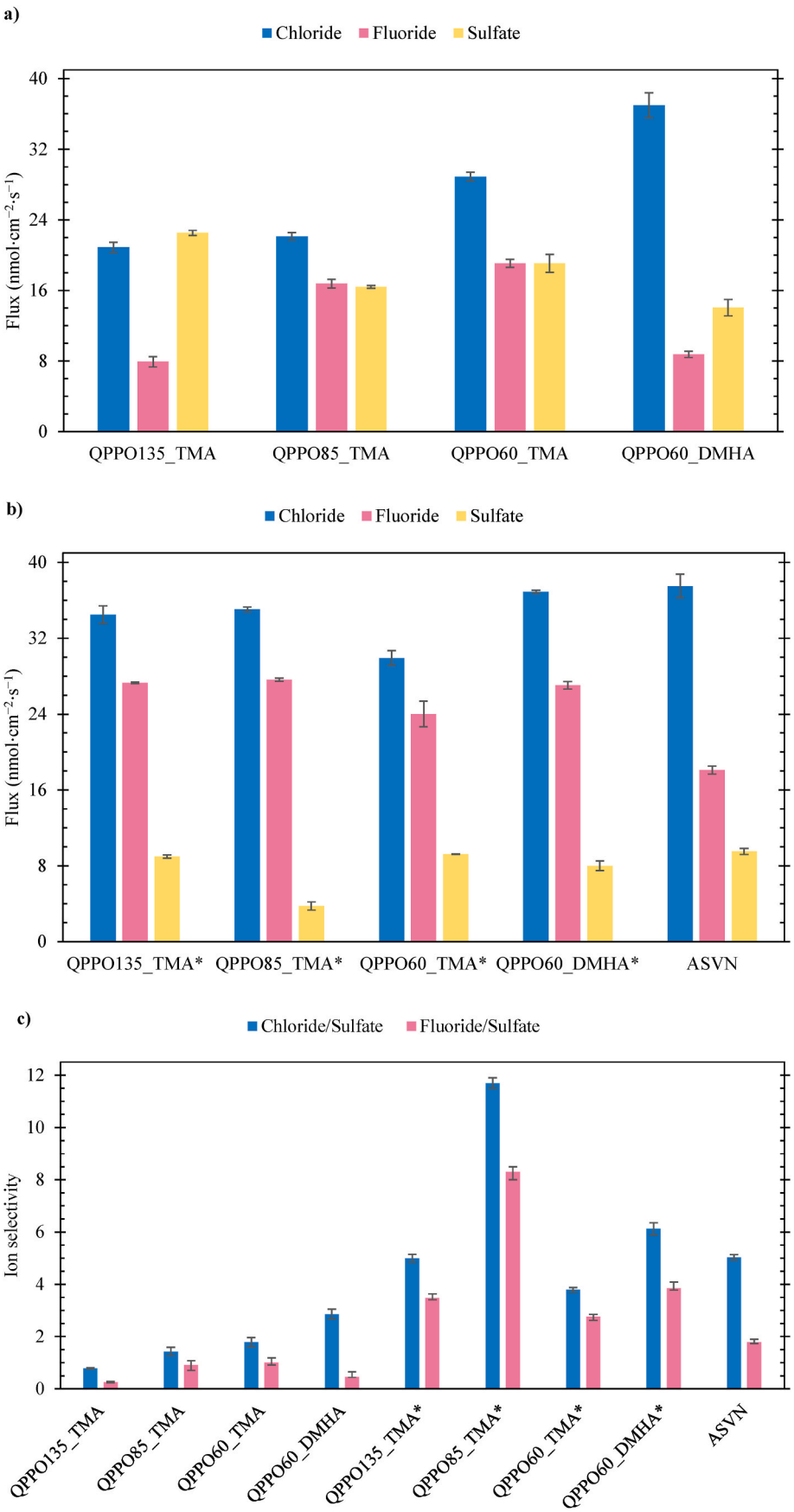

Fig. 8. a) Flux of unmodified AEMs; b) flux of modified and ASVN AEMs; c) ion selectivity of unmodified, modified and ASVN AEMs. The symbol * represents LbL-modified membranes: *i.e.*, QPPO135_TMA* = QPPO135_TMA_$(PSS/PAH)_{2.5}$.

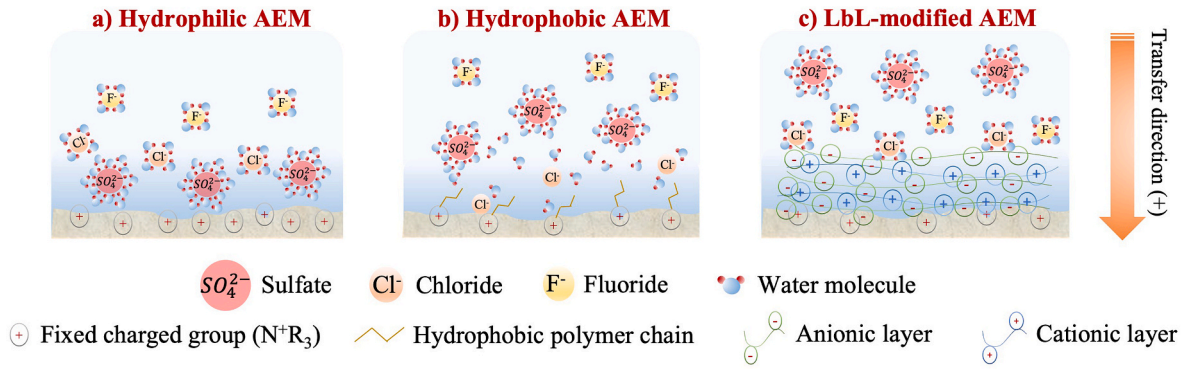

Scheme 3. Anion transport order: a) hydrophilic AEMs facilitate the transport of multivalent ions due to higher electrostatic affinity; b) hydrophobic AEMs retard the passage of ions with higher hydration energy which is unlikely to undergo dehydration compared to an ion with lower hydration energy which undergoes dehydration; c) imparting dense anionic layers impede the passage of multivalent ions due to higher electrostatic repulsion and size-exclusion effect.

transport of bigger ions. On the other hand, the hydrophobicity of the membrane negatively influenced the flux of F^- due to its strong water binding capability as SO_4^{2-} (Fig. 8a). In this case, Coulombic attraction between the opposite charge of fixed groups in the membrane and hydrophilic anions (F^- and SO_4^{2-}) becomes decisive in opposition to the case between Cl^- and SO_4^{2-}. Hence, F^- transport rate was surpassed by SO_4^{2-} anions. Consequently, the permeation rate of anions in a ternary mixture was observed as $Cl^- > SO_4^{2-} > F^-$ through the DMHA-based membrane (Scheme 3b). It is important to note that $Cl^-/\ SO_4^{2-}$ selectivity compromised FCC which increased with the hydrophobicity order of the membranes. Therefore, when the fractionation between ions possessing different dehydration capabilities is of interest (i.e., Cl^- and SO_4^{2-}), it is substantially critical to adjust the FCC of the membrane. However, no direct correlation was observed between the FCC and the transfer order of ions having similar hydration behavior (i.e., F^- and SO_4^{2-}), as dehydration is no longer a prevalent mechanism to define ion selectivity.

Surface modification was applied to enhance the separation performances of the developed membranes. AEMs were modified by 3 layers of PSS and 2 layers of PAH alternatively. Fig. 8b displays that the fluxes of monovalent anions were improved dramatically after the surface modification of the bare membranes, which also enhanced ion selectivity (Fig. 8c). The percent increase of monovalent selectivity is much higher for QPPO135_TMA and QPPO85_TMA than QPPO60_TMA and QPPO60_DMHA, which agrees well with the amount of deposition of polyelectrolyte layers confirmed by XPS measurements. Higher adsorption of polyelectrolytes on QPPO135_TMA and QPPO85_TMA membranes is owing to their high IEC values (>1.5 mmol g^{-1}), providing more excess free charge for the attachment of the polyelectrolyte segments. This brought about $Cl^-/\ SO_4^{2-}$ and $F^-/\ SO_4^{2-}$ selectivity of QPPO135_TMA to increase from 0.78 ± 0.02 and 0.26 ± 0.02 to 4.99 ± 0.15 and 3.48 ± 0.07 after only 5 layers of polyelectrolyte deposition. Nevertheless, the highest monovalent selectivity of $Cl^-/\ SO_4^{2-}$ (11.7 ± 0.2) and $F^-/\ SO_4^{2-}$ (8.3 ± 0.3) was achieved by QPPO85_TMA_$(PSS/PAH)_{2.5}$ despite its slightly less polyelectrolyte adsorption capability. The lower selectivity performance of QPPO135_TMA_$(PSS/PAH)_{2.5}$ can be explained by the relatively high IEC of its bare form, which causes high SR and oversized ion channels by the hydration of fixed charged groups in the membrane network facilitating the transport of bigger ions. Therefore, more deposition was required to sufficiently cover oversized sub-nanometer pores at the surface to reach the same level of selectivity performance of QPPO85_TMA_$(PSS/PAH)_{2.5}$. On the other hand, the bare QPPO85_TMA membrane restricted the passage of SO_4^{2-} more due to its denser structure, yielding higher monovalent selectivity even after the same number of polyelectrolyte deposition layers as the QPPO135_TMA membrane. Meanwhile, $Cl^-/\ SO_4^{2-}$ selectivity (5.03 ± 0.1) of ASVN was the same as the QPPO135_TMA_$(PSS/PAH)_{2.5}$ membrane, whereas the $F^-/\ SO_4^{2-}$ selectivity (1.79 ± 0.06) was found to be almost 50% lower.

When multilayers were formed on QPPO60_DMHA and QPPO60_TMA, the $Cl^-/\ SO_4^{2-}$ selectivity was 6.12 ± 0.23 and 3.79 ± 0.09, while the $F^-/\ SO_4^{2-}$ selectivity was 3.85 ± 0.07 and 2.76 ± 0.15, respectively. QPPO60_TMA_$(PSS/PAH)_{2.5}$ represented the least competitive ion selectivity performances among all developed membranes, which could be explained by a much lower elemental increase of N% and S% after LbL coating due to its lower IEC value (<0.9 mmol g^{-1}). Notwithstanding, QPPO60_DMHA_$(PSS/PAH)_{2.5}$ showed even higher monovalent selectivity than QPPO135_TMA_$(PSS/PAH)_{2.5}$ (Fig. 8c), which can be ascribed to the synergistic effects of the surface and network of the membrane. Notably, the increase in $Cl^-/\ SO_4^{2-}$ selectivity is much lower for QPPO60_DMHA than QPPO135_TMA after surface coating displaying the higher polyelectrolyte adsorption on QPPO135_TMA compared to QPPO60_DMHA with the same number of deposition layers which was also confirmed by the XPS measurements. However, the bare QPPO60_DMHA membrane displayed much higher resistance to the transfer of SO_4^{2-} than QPPO135_TMA which reduced the need for the high number of deposition layers to exceed the selectivity performance provided by QPPO135_TMA_$(PSS/PAH)_{2.5}$. On the other hand, the $F^-/\ SO_4^{2-}$ selectivity increase of QPPO60_DMHA was almost as high as QPPO135_TMA after the polyelectrolyte assembly. The reason is that hydration energy-related affinity between F^- and SO_4^{2-} anions and QPPO60_DMHA or QPPO135_TMA was not the main selectivity mechanism due to similar hydration behavior of the respective ions. Instead, electrostatic-based affinity was the dominant separation mechanism as a result of the valency difference. Therefore, F^- anions were surpassed by SO_4^{2-} through both hydrophilic and hydrophobic membranes. After surface modification, the affinity and ingress rate of ions of higher valency and bigger size was reduced due to higher Coulombic repulsion and denser layer formation, which led to a swap between SO_4^{2-} and F^- anions on the surface compared to their unmodified forms. In addition, the decreased water contact angle of modified membranes (Fig. 5) ruled out the negative effect of hydrophobic surface on the affinity of F^- anions. Hence, the flux of F^- was around 27 nmol cm^{-2} s^{-1} for the modified QPPO60_DMHA and QPPO135_TMA membranes. Therefore, the order of permeability was found as $Cl^- > F^- > SO_4^{2-}$ through all modified membranes (Scheme 3c). It is important to note that adequate fixed charged groups (>1.5 mmol g^{-1}) and moderate hydrophobicity of the membranes contributed to the ion selectivity most due to the most optimized microstructure and high enough polyelectrolyte adsorption.

Previously reported $Cl^-/\ SO_4^{2-}$ selectivity performances of LbL-modified AEMs are summarized in Table 6. The resulting monovalent

Table 6
Overview of Cl^-/SO_4^{2-} selectivity of LbL-modified membranes.

Bare AEM	Type of deposition	Polyanion	Polycation	# of layers	Feed solution	Ion selectivity	Ref
Fujifilm Type-1	Electrically aided	PDA	NSBC	3	0.02 M NaCl 0.02 M Na_2SO_4	2.2	[53]
Fujifilm Type-1	Electrically aided	PSS	HACC	18	0.02 M NaCl 0.02 M Na_2SO_4	2.9	[54]
Fujifilm Type-1	Electrically aided	PSS	HACC	9	0.05 M NaCl 0.05 M Na_2SO_4	5.1	[55]
Fujifilm Type-1	Electrically aided	PSSMA	HACC	15	0.05 M NaCl 0.05 M Na_2SO_4	4.9	[56]
Fujifilm Type-1	Electrically aided	PSSMA	HACC	11	0.05 M NaCl 0.05 M Na_2SO_4	2.2	[57]
Fujifilm Type-1	Static	PSS	PAH	11	0.01 M NaCl 0.01 M Na_2SO_4	7.4	[27]
TWEDA-1	Static	PSS	PDDA	11	0.01 M NaCl 0.01 M Na_2SO_4	11.5	[28]
NEOSEPTA AMX	Static	PSS	PAH	15	0.01 M NaCl 0.01 M Na_2SO_4	1.8	[58]
QPPO85_TMA	Static	PSS	PAH	5	0.01 M NaCl 0.01 M Na_2SO_4	11.7 ± 0.2	This work

selectivities range from 1.82 to 11.5 for either statically or electrically modified commercial AEMs. High monovalent selectivities were achieved after a high deposition number of layers (>10) due to the properties of the commercial membranes. This list reveals the importance of substrate design to offer enhanced selectivity and limit the number of deposition layers. Moreover, to the best of our knowledge, F/SO_4^{2-} selectivity of tailor-made membranes has so far only been explored in a recent study by Zhao et al. [7]. Novel kevlar amide nanofiber-based AEM was synthesized with hydroxypropyltrimethyl ammonium chloride chitosan (HACC) for F^- removal. Achieved F^-/SO_4^{2-} selectivity was represented as 2.75. $SO_4^{2-}F^-$r. In our work, single-stage ED using as-prepared QPPO85_TMA exhibits a relatively high Cl^-/SO_4^{2-} (11.7 ± 0.2) and F^-/SO_4^{2-} (8.3 ± 0.3) selectivities after only 5 layers of polyelectrolyte deposition. It is also noteworthy that the equivalent concentration ratios of all anions were the same which was a more challenging condition for the fractionation of F^- in the presence of Cl^- and SO_4^{2-} [4].

The energy consumption and the Gibbs free energy of mixing were calculated to illustrate the spent energy and the minimum theoretical energy required to separate ions (Fig. S11). The energy consumption of bare AEMs was much higher than that of modified AEMs indicating that the energy consumption was consistent with flux and ion selectivity performances [38,59]. Remarkably, QPPO85_TMA_$(PSS/PAH)_{2.5,}$ displaying the highest monovalent selectivity performance among all synthesized membranes, needed the least energy. Moreover, the energy demand for the separation of anions through modified membranes approached the thermodynamic minimum. This shows that not only are mechanistic capabilities improved but also the energy footprint during operation is much better. These small-scale experiments indicate an energy consumption reduction of a factor of two or more.

4. Conclusions

Simultaneous separation of Cl^- and F^- anions over SO_4^{2-} through developed AEMs was demonstrated in an equimolar ternary mixture using ED. Bare AEMs were prepared directly from the quaternization reaction between brominated polymers and tertiary amines. LbL assembly was successfully applied on AEMs confirmed by XPS and water contact angle measurements. The microstructure of the membranes was adjusted by both the bromination reaction and the type of tertiary amines influencing the extent of ion selectivity and water transfer. When the membrane had relatively high IEC, the transport rate of Cl^- and F^- anions were impeded by SO_4^{2-} anions that transfer easily through wide hydrophilic entrances and create higher electrostatic affinity with fixed charged groups in the membrane. The order of ion permeation was $SO_4^{2-} > Cl^- > F^-$, which did not propose monovalent selectivity. Increasing the chain length of the alkyl side provided the highest FCC, which played a crucial role in the selectivity of ions of different hydration behavior (Cl^-/SO_4^{2-}). However, the dehydration phenomenon was no longer the main parameter to explain the selectivity of F^-/SO_4^{2-} due to the similar hydration behavior of the respective ions, which was overruled by electrostatic affinity in favor of SO_4^{2-}. Hence, the order of ion permeation through hydrophobic membranes was demonstrated as $Cl^- > SO_4^{2-} > F^-$.

Monovalent selectivity performances were boosted after LbL modification on the bare membranes. PSS-terminated membranes impeded the passage of SO_4^{2-} anions due to the charge repulsion effect. Furthermore, the improved compactness of the membrane after deposition enhanced the ion selectivity by size-exclusion effect, hindering ions with bigger hydrated ionic radii from passing through the membrane. Therefore, the synergistic effect of electrostatic interaction and dense layer altered the localization of anions at the interface after modification. All modified membranes represented the permeation rate as $Cl^- > F^- > SO_4^{2-}$. The extent of monovalent selectivity varied among modified AEMs, depending on the characteristics of the bare membrane (*i.e.* IEC, hydrophobicity). In addition, relatively higher Cl^-/SO_4^{2-} and F^-/SO_4^{2-} selectivity performances were achieved compared to commercial monovalent selective ASVN membrane. It was also observed that the tailor-made monovalent selective membranes demonstrated significantly lower energy consumption per mole of Cl^- and F^- ions than their bare form.

Based on the experiments, it is reasonable to conclude that ion selectivity through dense membranes can be improved by simultaneously optimizing the membranes' structural and surface properties, which are decisive elements for the transport of respective ions, since the surface modification influenced the ions' affinity and ingress rate, while the network of bare membranes affected their mobility and interaction with fixed charge groups in the membrane. Significant findings regarding the ion selectivity concept can be summarized as follows:

i) hydrophobic membranes deposited by the polyelectrolyte layers provide high monovalent selectivity performances, but higher selectivity values might be limited by the polyelectrolyte deposition capacity due to the low IEC of the bare membrane,
ii) hydrophilic membranes modified by polyelectrolyte layers achieve high monovalent selectivity performances, but higher monovalent selectivity is restricted by the limited number of

deposition layers due to the insufficient coverage of the wide hydrophilic entrances of the bare membrane,

iii) bare membranes having moderate IEC and WU values are the most promising candidates for the highest monovalent selectivity with a relatively low number of deposition layers due to enabling high enough polyelectrolyte adsorption capacity and compact microstructure,

iv) the simultaneous adjustment of the network and surface may have a dual effect for higher selectivity performances of chemically and physically similar ions,

v) lower energy consumption and cost of production as well as the sustainability of the process can be achieved if a relatively low number of deposition layers in the AEM membrane is sufficient for the separation.

In future studies, the stability of the modified membranes and the effect of process conditions (*e.g.,* current density and flow rate) should be examined in detail for long-term operation and further improved selectivity.

Author statement

Önder Tekinalp: Conceptualization, Methodology, Formal analysis, Validation, Investigation, Writing - original draft, Visualization.

Pauline Zimmermann: Writing - Review & editing.

Odne Stokke Burheim: Supervision, Writing - Review & editing.

Liyuan Deng: Conceptualization, Supervision, Writing - Review & editing. All authors have read and agreed to the published version of the manuscript.

Declaration of competing interest

The authors declare that they have no known competing financial interests or personal relationships that could have appeared to influence the work reported in this paper.

Data availability

Data will be made available on request.

Acknowledgements

The authors acknowledge the financial support from the Research Council of Norway (RCN-BIA) through the PRICE project (No. 294543) and the support to the Norwegian Micro- and Nano-Fabrication Facility, NorFab (No. 295864). The authors also thank S. Menegatti and other colleagues from Boliden Odda AS for technical assistance.

Nomenclature

λ	hydration number
^{1}H NMR	^{1}H nuclear magnetic resonance
AEM	anion exchange membrane
$AgNO_3$	silver nitrate
AIBN	2,2′-Azobisisobutyronitrile
BPPO	brominated poly(2,6- dimethyl-1,4-phenylene oxide)
$CDCl_3$	deuterated chloroform
CEM	cation exchange membrane
DB	degree of bromination
DMHA	dimethylhexylamine
DMSO-d_6	dimethyl sulfoxide
ED	electrodialysis
EWT	electroosmotic water transfer
FCC	fixed charge concentration
FT-IR	fourier transform infrared spectroscopy
HACC	hydroxypropyltrimethyl ammonium chloride chitosan
HCl	hydrochloric acid
IEC	ion exchange capacity
IEM	ion exchange membrane
LbL	layer-by-layer
Na_2SO_4	sodium sulfate
NaCl	sodium chloride
NaF	sodium fluoride
NaOH	sodium hydroxide
NBS	N-bromosuccinimide
NMP	N-methyl-2-pyrrolidone
NSBC	N–O-sulfonic acid benzyl chitosan
PAH	poly(allylamine hydrochloride)
PDA	polydopamine
PPO	poly(2,6- dimethyl-1,4-phenylene oxide)
PSS	poly (sodium 4-styrenesulfonate)
PSSMA	sodium salt of poly(4-styrenesulfonicacid-co-maleicacid) sodium salt
QPPO	quaternized poly(2,6- dimethyl-1,4-phenylene oxide)
TMA	trimethylamine
WU	water uptake
XPS	x-ray photoelectron spectroscopy

Appendix A. Supplementary data

Supplementary data to this article can be found online at https://doi.org/10.1016/j.memsci.2022.121148.

References

[1] Y. Li, Z. Yang, K. Yang, J. Wei, Z. Li, C. Ma, X. Yang, T. Wang, G. Zeng, G. Yu, Z. Yu, C. Zhang, Removal of chloride from water and wastewater: removal mechanisms and recent trends, Sci. Total Environ. 821 (2022), 153174, https://doi.org/10.1016/j.scitotenv.2022.153174.

[2] Z. Luo, D. Wang, D. Zhu, J. Xu, H. Jiang, W. Geng, W. Wei, Z. Lian, Separation of fluoride and chloride ions from ammonia-based flue gas desulfurization slurry using a two-stage electrodialysis, Chem. Eng. Res. Des. 147 (2019) 73–82, https://doi.org/10.1016/j.cherd.2019.05.003.

[3] M. Stevens, B. Batlokwa, Removal of excess toxic chloride and fluoride anions from wastewater employing eggshells waste remains, Int. J. Adv. Eng. Res. Sci. 5 (2018) 79–80, https://doi.org/10.22161/ijaers.5.9.9.

[4] M. Grzegorzek, K. Majewska-Nowak, A.E. Ahmed, Removal of fluoride from multicomponent water solutions with the use of monovalent selective ion-exchange membranes, Sci. Total Environ. 722 (2020), 137681, https://doi.org/10.1016/j.scitotenv.2020.137681.

[5] H. Strathmann, Electrodialysis, a mature technology with a multitude of new applications, Desalination 264 (2010) 268–288, https://doi.org/10.1016/j.desal.2010.04.069.

[6] C. Huang, T. Xu, Y. Zhang, Y. Xue, G. Chen, Application of electrodialysis to the production of organic acids : state-of-the-art and recent developments, J. Membr. Sci. 288 (2007) 1–12, https://doi.org/10.1016/j.memsci.2006.11.026.

[7] Y. Zhao, W. Lu, N. Mamrol, T. Croes, Z. Mai, S. Houtmeyers, R. Dewil, Y. Zhang, X. Yang, B. Van der Bruggen, Self-assembled embedding of ion exchange materials into nanofiber-based hydrogel framework for fluoride capture, Chem. Eng. J. 431 (2022), 134201, https://doi.org/10.1016/j.cej.2021.134201.

[8] P. Pillai, S. Dharaskar, S. Pandian, H. Panchal, Overview of fluoride removal from water using separation techniques, Environ. Technol. Innovat. 21 (2021), 101246, https://doi.org/10.1016/j.eti.2020.101246.

[9] L. Ge, B. Wu, D. Yu, A.N. Mondal, L. Hou, N.U. Afsar, Q. Li, T. Xu, J. Miao, T. Xu, Monovalent cation perm-selective membranes (MCPMs): new developments and perspectives, Chin. J. Chem. Eng. 25 (2017) 1606–1615, https://doi.org/10.1016/j.cjche.2017.06.002.

[10] T. Sata, Studies on anion exchange membranes having permselectivity for specific anions in electrodialysis - effect of hydrophilicity of anion exchange membranes on permselectivity of anions, J. Membr. Sci. 167 (2000) 1–31, https://doi.org/10.1016/S0376-7388(99)00277-X.

[11] R. Epsztein, R.M. DuChanois, C.L. Ritt, A. Noy, M. Elimelech, Towards single-species selectivity of membranes with subnanometre pores, Nat. Nanotechnol. 15 (2020) 426–436, https://doi.org/10.1038/s41565-020-0713-6.

[12] E.R. Nightingale, Phenomenological theory of ion solvation. Effective radii of hydrated ions, J. Phys. Chem. 63 (1959) 1381–1387, https://doi.org/10.1021/j150579a011.

[13] G. Rayner-canham, T. Overton, Descriptive Inorganic Chemistry, fifth ed., W. H. Freeman and Company, New York, 2009.

[14] Y. Marcus, Thermodynamics of solvation of ions, J. Chem. Soc., Faraday Trans. 89 (1993) 713–718, https://doi.org/10.1017/CBO9781107415324.004.

[15] X. Zhou, Z. Wang, R. Epsztein, C. Zhan, W. Li, J.D. Fortner, T.A. Pham, J.H. Kim, M. Elimelech, Intrapore energy barriers govern ion transport and selectivity of

desalination membranes, Sci. Adv. 6 (2020) 1–10, https://doi.org/10.1126/sciadv.abd9045.
[16] W. Ji, B. Wu, Y. Zhu, M. Irfan, N. Ul Afsar, L. Ge, T. Xu, Self-organized nanostructured anion exchange membranes for acid recovery, Chem. Eng. J. 382 (2020), 122838, https://doi.org/10.1016/j.cej.2019.122838.
[17] J. Liao, X. Yu, Q. Chen, X. Gao, H. Ruan, J. Shen, C. Gao, Monovalent anion selective anion-exchange membranes with imidazolium salt-terminated side-chains: investigating the effect of hydrophobic alkyl spacer length, J. Membr. Sci. 599 (2020), 117818, https://doi.org/10.1016/j.memsci.2020.117818.
[18] X. Wang, X. Zhang, C. Wu, X. Han, C. Xu, Anion exchange membranes with excellent monovalent anion perm-selectivity for electrodialysis applications, Chem. Eng. Res. Des. 158 (2020) 24–32, https://doi.org/10.1016/j.cherd.2020.03.021.
[19] J. Liao, J. Zhu, S. Yang, N. Pan, X. Yu, C. Wang, J. Li, J. Shen, Long-side-chain type imidazolium-functionalized fluoro-methyl poly(arylene ether ketone) anion exchange membranes with superior electrodialysis performance, J. Membr. Sci. 574 (2019) 181–195, https://doi.org/10.1016/j.memsci.2018.12.066.
[20] M. Irfan, L. Ge, Y. Wang, Z. Yang, T. Xu, Hydrophobic side chains impart anion exchange membranes with high monovalent-divalent anion selectivity in electrodialysis, ACS Sustain. Chem. Eng. 7 (2019) 4429–4442, https://doi.org/10.1021/acssuschemeng.8b06426.
[21] J. Liao, X. Yu, N. Pan, J. Li, J. Shen, C. Gao, Amphoteric ion-exchange membranes with superior mono-/bi-valent anion separation performance for electrodialysis applications, J. Membr. Sci. 577 (2019) 153–164, https://doi.org/10.1016/j.memsci.2019.01.052.
[22] C. Wang, N. Pan, J. Liao, H. Ruan, A. Sotto, J. Shen, Effect of microstructures of side-chain-type Anion exchange membranes on mono-/bivalent anion permselectivity in electrodialysis, ACS Appl. Polym. Mater. 3 (2021) 342–353, https://doi.org/10.1021/acsapm.0c01133.
[23] T. Sata, T. Yamaguchi, K. Matsusaki, Effect of hydrophobicity of ion exchange groups of anion exchange membranes on permselectivity between two anions, J. Phys. Chem. 99 (1995) 12875–12882, https://doi.org/10.1021/j100034a028.
[24] T. Luo, S. Abdu, M. Wessling, Selectivity of ion exchange membranes: a review, J. Membr. Sci. 555 (2018) 429–454, https://doi.org/10.1016/j.memsci.2018.03.051.
[25] J. Ran, L. Wu, Y. He, Z. Yang, Y. Wang, C. Jiang, L. Ge, E. Bakangura, T. Xu, Ion exchange membranes: new developments and applications, J. Membr. Sci. 522 (2017) 267–291, https://doi.org/10.1016/j.memsci.2016.09.033.
[26] Ö. Tekinalp, S. Alsoy Altinkaya, Development of high flux nanofiltration membranes through single bilayer polyethyleneimine/alginate deposition, J. Colloid Interface Sci. 537 (2019) 215–227, https://doi.org/10.1016/j.jcis.2018.10.089.
[27] M. Ahmad, C. Tang, L. Yang, A. Yaroshchuk, M.L. Bruening, Layer-by-layer modification of aliphatic polyamide anion-exchange membranes to increase Cl−/SO42− selectivity, J. Membr. Sci. 578 (2019) 209–219, https://doi.org/10.1016/j.memsci.2019.02.018.
[28] Y. Zhang, R. Liu, Q. Lang, M. Tan, Y. Zhang, Composite anion exchange membrane made by layer-by-layer method for selective ion separation and water migration control, Separ. Purif. Technol. 192 (2018) 278–286, https://doi.org/10.1016/j.seppur.2017.10.022.
[29] T. Rijnaarts, D.M. Reurink, F. Radmanesh, W.M. de Vos, K. Nijmeijer, Layer-by-layer coatings on ion exchange membranes: effect of multilayer charge and hydration on monovalent ion selectivities, J. Membr. Sci. 570–571 (2019) 513–521, https://doi.org/10.1016/j.memsci.2018.10.074.
[30] N. Kabay, Ö. Arar, S. Samatya, Ü. Yüksel, M. Yüksel, Separation of fluoride from aqueous solution by electrodialysis: effect of process parameters and other ionic species, J. Hazard Mater. 153 (2008) 107–113, https://doi.org/10.1016/j.jhazmat.2007.08.024.
[31] O. Arar, E. Yavuz, U. Yuksel, N. Kabay, Separation of low concentration of fluoride from water by electrodialysis (ED) in the presence of chloride and sulfate ions, Separ. Sci. Technol. 44 (2009) 1562–1573, https://doi.org/10.1080/01496390902775943.
[32] E. Ergun, A. Tor, Y. Cengeloglu, I. Kocak, Electrodialytic removal of fluoride from water: effects of process parameters and accompanying anions, Separ. Purif. Technol. 64 (2008) 147–153, https://doi.org/10.1016/j.seppur.2008.09.009.
[33] S. Willdorf-Cohen, A.N. Mondal, D.R. Dekel, C.E. Diesendruck, Chemical stability of poly(phenylene oxide)-based ionomers in an anion exchange-membrane fuel cell environment, J. Mater. Chem. A. 6 (2018) 22234–22239, https://doi.org/10.1039/C8TA05785K.
[34] T. Xu, Z. Liu, W. Yang, Fundamental studies of a new series of anion exchange membranes: membrane prepared from poly(2,6-dimethyl-1,4-phenylene oxide) (PPO) and triethylamine, J. Membr. Sci. 249 (2005) 183–191, https://doi.org/10.1016/j.memsci.2004.10.010.
[35] J. Parrondo, V. Ramani, Stability of poly(2,6-dimethyl 1,4-phenylene)Oxide-Based anion exchange membrane separator and solubilized electrode binder in solid-state alkaline water electrolyzers, J. Electrochem. Soc. 161 (2014) F1015–F1020, https://doi.org/10.1149/2.0601410jes.
[36] L. Hao, J. Liao, Y. Liu, H. Ruan, A. Sotto, B. Van der Bruggen, J. Shen, Highly conductive anion exchange membranes with low water uptake and performance evaluation in electrodialysis, Separ. Purif. Technol. 211 (2019) 481–490, https://doi.org/10.1016/j.seppur.2018.09.042.
[37] B. Wei, J. Pan, J. Feng, C. Chen, S. Liao, Y. Yu, X. Li, Highly conductive and permselective anion exchange membranes for electrodialysis desalination with series-connected dications appending flexible hydrophobic tails, Desalination 474 (2020), 114184, https://doi.org/10.1016/j.desal.2019.114184.
[38] S. Abdu, M.C. Martí-Calatayud, J.E. Wong, M. García-Gabaldón, M. Wessling, Layer-by-layer modification of cation exchange membranes controls ion selectivity and water splitting, ACS Appl. Mater. Interfaces 6 (2014) 1843–1854, https://doi.org/10.1021/am4048317.
[39] P. Atkins, J. Paulo de, Atkins' Physical Chemistry, Oxford University Press, 2006.
[40] S.H. Roh, M.H. Lim, T. Sadhasivam, H.Y. Jung, Investigation on physico-chemical and electrochemical performance of poly(phenylene oxide)-based anion exchange membrane for vanadium redox flow battery systems, Electrochim. Acta 325 (2019), 134944, https://doi.org/10.1016/j.electacta.2019.134944.
[41] J. Pan, J. Ding, R. Tan, G. Chen, Y. Zhao, C. Gao, B. Van der Bruggen, J. Shen, Preparation of a monovalent selective anion exchange membrane through constructing a covalently crosslinked interface by electro-deposition of polyethyleneimine, J. Membr. Sci. 539 (2017) 263–272, https://doi.org/10.1016/j.memsci.2017.06.017.
[42] P. Zimmermann, S.B.B. Solberg, Ö. Tekinalp, J.J. Lamb, Ø. Wilhelmsen, L. Deng, O. S. Burheim, Heat to hydrogen by RED—reviewing membranes and salts for the RED heat engine concept, Membranes 12 (2022), https://doi.org/10.3390/membranes12010048.
[43] X. Tongwen, F.F. Zha, Fundamental studies on a new series of anion exchange membranes: effect of simultaneous amination-crosslinking processes on membranes ion-exchange capacity and dimensional stability, J. Membr. Sci. 199 (2002) 203–210, https://doi.org/10.1016/S0376-7388(01)00698-6.
[44] F.A. de Bruijn, R.C. Makkus, R.K.A.M. Mallant, G.J.M. Janssen, Chapter Five Materials for State-Of-The-Art PEM Fuel Cells, and Their Suitability for Operation above 100°C, 2007, https://doi.org/10.1016/S1752-301X(07)80010-X.
[45] R. Epsztein, E. Shaulsky, M. Qin, M. Elimelech, Activation behavior for ion permeation in ion-exchange membranes: role of ion dehydration in selective transport, J. Membr. Sci. 580 (2019) 316–326, https://doi.org/10.1016/j.memsci.2019.02.009.
[46] M. Tedesco, H.V.M. Hamelers, P.M. Biesheuvel, Nernst-Planck transport theory for (reverse) electrodialysis: II. Effect of water transport through ion-exchange membranes, J. Membr. Sci. 531 (2017) 172–182, https://doi.org/10.1016/j.memsci.2017.02.031.
[47] V.K. Indusekhar, N. Krishnaswamy, Water transport studies on interpolymer ion-exchange membranes, Desalination 52 (1985) 309–316, https://doi.org/10.1016/0011-9164(85)80040-0.
[48] L. Han, S. Galier, H. Roux-de Balmann, Ion hydration number and electro-osmosis during electrodialysis of mixed salt solution, Desalination 373 (2015) 38–46, https://doi.org/10.1016/j.desal.2015.06.023.
[49] W. Jin, A. Toutianoush, B. Tieke, Size- and charge-selective transport of aromatic compounds across polyelectrolyte multilayer membranes, Appl. Surf. Sci. 246 (2005) 444–450, https://doi.org/10.1016/j.apsusc.2004.11.067.
[50] W. Cheng, C. Liu, T. Tong, R. Epsztein, M. Sun, R. Verduzco, J. Ma, M. Elimelech, Selective removal of divalent cations by polyelectrolyte multilayer nanofiltration membrane: role of polyelectrolyte charge, ion size, and ionic strength, J. Membr. Sci. 559 (2018) 98–106, https://doi.org/10.1016/j.memsci.2018.04.052.
[51] X. Pang, Y. Tao, Y. Xu, J. Pan, J. Shen, C. Gao, Enhanced monovalent selectivity of cation exchange membranes via adjustable charge density on functional layers, J. Membr. Sci. 595 (2020), 117544, https://doi.org/10.1016/j.memsci.2019.117544.
[52] R. Epsztein, E. Shaulsky, N. Dizge, D.M. Warsinger, M. Elimelech, Role of ionic charge density in donnan exclusion of monovalent anions by nanofiltration, Environ. Sci. Technol. 52 (2018) 4108–4116, https://doi.org/10.1021/acs.est.7b06400.
[53] Y. Zhao, H. Liu, K. Tang, Y. Jin, J. Pan, B. Van Der Bruggen, J. Shen, C. Gao, Mimicking the cell membrane: bio-inspired simultaneous functions with monovalent anion selectivity and antifouling properties of anion exchange membrane, Sci. Rep. 6 (2016) 1–13, https://doi.org/10.1038/srep37285.
[54] Y. Zhao, K. Tang, H. Liu, B. Van der Bruggen, A. Sotto Díaz, J. Shen, C. Gao, An anion exchange membrane modified by alternate electro-deposition layers with enhanced monovalent selectivity, J. Membr. Sci. 520 (2016) 262–271, https://doi.org/10.1016/j.memsci.2016.07.026.
[55] L. Hao, J. Liao, Y. Jiang, J. Zhu, J. Li, Y. Zhao, "Sandwich"-like structure modified anion exchange membrane with enhanced monovalent selectivity and fouling resistant, J. Membr. Sci. 556 (2018) 98–106, https://doi.org/10.1016/j.memsci.2018.03.082.
[56] Y. Zhao, C. Gao, B. Van Der Bruggen, Technology-driven layer-by-layer assembly of a membrane for selective separation of monovalent anions and antifouling, Nanoscale 11 (2019) 2264–2274, https://doi.org/10.1039/c8nr09086f.
[57] Y. Lan, Y. Huang, H. Qi, L. Lai, L. Xia, Z. Zhao, Y. Zhao, Alternating electric field-based ionic control and layer-by-layer assembly of anion exchange membranes for enhancing target anion selectivity, Desalination 533 (2022), 115773, https://doi.org/10.1016/j.desal.2022.115773.
[58] S. Mulyati, R. Takagi, A. Fujii, Y. Ohmukai, H. Matsuyama, Simultaneous improvement of the monovalent anion selectivity and antifouling properties of an anion exchange membrane in an electrodialysis process, using polyelectrolyte multilayer deposition, J. Membr. Sci. 431 (2013) 113–120, https://doi.org/10.1016/j.memsci.2012.12.022.
[59] S. Yang, Y. Liu, J. Liao, H. Liu, Y. Jiang, B. Van Der Bruggen, J. Shen, C. Gao, Codeposition modification of cation exchange membranes with dopamine and crown ether to achieve high K+ electrodialysis selectivity, ACS Appl. Mater. Interfaces 11 (2019) 17730–17741, https://doi.org/10.1021/acsami.8b21031.